2360 *Inorg. Chem.* **2000,** *39,* 2360−2366

Experimental Electron Density Analysis of $Mn_2(CO)_{10}$: Metal−Metal and Metal−Ligand Bond Characterization

Riccardo Bianchi,[†] **Giuliana Gervasio,**[*,‡] **and Domenica Marabello**[‡]

Centro CNR per lo Studio delle Relazioni tra Struttura e Reattività Chimica, Via Venezian 21, 20133
Milano, Italy, and Dipartimento di Chimica I.F.M. dell'Università, Via P. Giuria 7, 10125 Torino, Italy

Received November 10, 1999

The experimental electron density $\rho(\mathbf{r})$ of $Mn_2(CO)_{10}$ was determined by a multipole analysis of accurate X-ray diffraction data at 120 K. The quantum theory of atoms in molecules (QTAM) was applied to $\rho(\mathbf{r})$ and its Laplacian $\nabla^2\rho(\mathbf{r})$. The QTAM analysis of $\rho(\mathbf{r})$ showed the presence of a bond critical point ($\mathbf{r}_c$); its associated bond path connects the two Mn atoms, but no cross interaction line was found between one manganese and the equatorial carbonyls of the other. The distribution of $\nabla^2\rho(\mathbf{r})$ indicated "closed-shell" interactions for the *metallic* Mn−Mn bond and the *dative* Mn−CO bonds. The values of the topological parameters of the density at $\mathbf{r}_c$, $\rho(\mathbf{r}_c)$, $\nabla^2\rho(\mathbf{r}_c)$, $G(\mathbf{r}_c)$ (kinetic energy density), and $V(\mathbf{r}_c)$ (potential energy density), characterize the bonds and are intermediate to those corresponding to typical ionic and covalent bonds.

Introduction

Manganese is a metal with a wide set of oxidation numbers ranging from −1 to +7 and forms complexes with charged or neutral ligands. Our attention was focused on the complex $Mn_2(CO)_{10}$, where the oxidation number of manganese is zero and the ligand is a neutral molecule. Cleavage of metal−metal bonds and metal−carbonyl bonds is found throughout organometallic chemistry, and therefore, accurate descriptions of these bonds are important for an understanding of organometallic reaction mechanisms.

$Mn_2(CO)_{10}$, one of the simplest binuclear carbonyls,[1] can be considered a prototype for some organometallics of higher nuclearity. It has a rich photochemistry,[2] and during its photolysis two primary photochemical reaction pathways are established:[3] metal−metal bond cleavage and dissociative loss of CO without metal−metal bond cleavage. Because of breaking of the metal−metal bond, $Mn_2(CO)_{10}$ acts as a catalyst in the ring opening of β-propiothiolactones[4] and its phosphine derivatives act as catalysts in homogeneous hydrogenation reactions.[5] Some compounds obtained from the breaking of the Mn−Mn bond in $Mn_2(CO)_{10}$ have been taken as models of intermediates in organic reactions[6] where transition metal−C,H bonds are formed.

Many theoretical[7] studies have been undertaken to provide accurate bond strength data regarding $Mn_2(CO)_{10}$ and its derivatives. Experimental deformation maps,[8a] electronic and vibrational spectroscopy data,[8b−f] some reaction mechanisms of $Mn_2(CO)_{10}$, and Mn−Mn bond dissociation entalpies[9] are reported elsewhere.

In all the cited papers, the Mn−Mn bond and Mn−CO bonds are, respectively, described according to MO formalism as a single σ bond and by the Dewar−Chatt−Duncanson model. Furthermore, some theoretical papers emphasize the presence of an additional bond between Mn and CO_{eq} of the other Mn.[7a,f,8a] However, there is no experimental evidence supporting the existence of this bond.[8a]

In this paper we complete the study[10] of the metal−metal and metal−ligand bonds of $Mn_2(CO)_{10}$ in terms of the topological properties[11] of experimental electron density, determined by a multipole refinement procedure.[12] A topological analysis of

---

[*] To whom correspondence should be addressed. Phone: (+39) 011 6707504. Fax: (+39) 011 6707855. E-mail: gervasio@ch.unito.it.

[†] Centro CNR per lo Studio delle Relazioni tra Struttura e Reattività Chimica

[‡] Dipartimento di Chimica I.F.M. dell'Università.

(1) (a) Dahl, L. F.; Ishishi, E.; Rundle, R. E. *J. Chem. Phys*. **1957**, *26*, 1750−1751. (b) Dahl, L. F.; Rundle, R. E. *Acta Crystallogr*. **1963**, *16*, 419−426. (c) Almenningen, A.; Jacobsen, G. G.; Seip, H. M. *Acta Chem. Scand*. **1969**, *23*, 685−686.

(2) (a) Geoffroy, G. L.; Wrighton, M. S. *Organometallic Photochemistry*; Academic Press: New York, 1979. (b) Geoffroy, G. L. *J. Chem. Educ.* **1983**, *60*, 861−866.

(3) (a) Rosa, A.; Ricciardi, G.; Baerends, E. J.; Stufkens, D. J. *Inorg. Chem*. **1995**, *34*, 3425−3432. (b) Rosa, A.; Ricciardi, G.; Baerends, E. J.; Stufkens, D. J. *Inorg. Chem*. **1996**, *35*, 2886−2897 and references therein.

(4) Adams, R. D.; Huang, M.; Huang, W. *Organometallics* **1997**, *16*, 4479−4485.

(5) Giordano, R.; Sappa, E.; Tiripicchio, A.; Tiripicchio Camellini, M.; Mays, M. J.; Brown, M. P. *Polyhedron* **1989**, *8*, 1855−1856.

(6) Folga, E.; Ziegler, T. *J. Am. Chem. Soc.* **1993**, *115*, 5169−5176.

(7) (a) Brown, D. A.; Chambers, W. J.; Fitzpatrick, N. J.; Rawlinson, S. R. M. *J. Chem. Soc. A* **1971**, 720−725. (b) Heijser, W.; Baerends, E. J.; Ros, P. *Discuss Faraday Soc. (Symp.)* **1980**, *14*, 211−234. (c) Levenson, R. A.; Gray, H. B. *J. Am. Chem. Soc.* **1975**, *97*, 6042−6047. (d) Elian, M.; Hoffmann, R. *Inorg. Chem.* **1975**, *14*, 1058−1076. (e) Nakatsuji, H.; Hada, M.; Kawashima, A. *Inorg. Chem.* **1992**, *31*, 1740−1744. (f) Veillard, A.; Rohmer, M.-M. *Int. J. Quantum Chem.* **1992**, *42*, 965−976. (g) Decker, S. A.; Donini, O.; Klobukowski, M. *J. Phys. Chem. A* **1997**, *101*, 8734−8740. (h) Liddel, M. J. *J. Organomet. Chem*. **1998**, *565*, 271−277. (i) MacDougall, P. J. The Laplacian of the electronic charge distribution. Ph.D. Thesis, Department of Chemistry, McMaster University, Hamilton, Ontario, Canada, 1989.

(8) (a) Martin, M.; Rees, B.; Mitschler, A. *Acta Crystallogr*. **1982**, *B38*, 6−15. (b) Bor, G.; Sbrignadello, G. *J. Chem. Soc., Dalton Trans*. **1974**, 440−448. (c) Levenson, R. A.; Gray, H. B.; Ceasar, G. P. *J. Am. Chem. Soc*. **1970**, *92*, 3653−3658. (d) Jones, L. H.; McDowell, R. S.; Goldblatt, M. *Inorg. Chem*. **1969**, *8*, 2349−2363. (e) Quicksall, C. O.; Spiro, T. G. *Inorg. Chem*. **1969**, *8*, 2363−2367. (f) Spiro, T. G. *Progr. Inorg. Chem*. **1970**, *11*, 1−51.

(9) Haines, L. I. B.; Hopgood, D.; Poë, A. J. *J. Chem. Soc. A* **1968**, 421−428.

(10) Bianchi, R.; Gervasio, G.; Marabello, D. *Chem. Commun*. **1998**, 1535−1536.

(11) (a) Bader, R. F. W. *Atoms in molecules—a Quantum Theory*; Oxford University Press: Oxford, 1990. (b) Bader, R. F. W. *J. Phys. Chem. A* **1998**, *102*, 7314−7323. (c) Bader, R. F. W.; MacDougall, P. J.; Lau, C. D. H. *J. Am. Chem. Soc*. **1984**, *106*, 1594−1605.

(12) Stewart, R. F. *Acta Crystallogr*. **1976**, *A32*, 565−574.

10.1021/ic991316e CCC: \$19.00

Table 1. Crystal Data for $Mn_2(CO)_{10}$ at 120 K

empirical formula	$Mn_2C_{10}O_{10}$
fw (amu)	389.98
lattice type, space group	monoclinic, $C2/c$
a (Å)	$a = 17.314(4)$
b (Å)	$b = 6.898(1)$
c (Å)	$c = 14.110(3)$
β (deg)	$\beta = 126.94(3)$
vol, Z (no. molecules in unit cell)	1346.9(5) Å^3, 4
density (calculated) (g/cm^3)	1.92
$F(000)$	760
abs coeff (mm^{-1})	1.92

the theoretical electron density for some mononuclear[13a] and binuclear[13b] carbonyls has already appeared.

Few papers report the topological characteristics of the experimental electron density of organometallic or coordination complexes[14] and, in particular, of bimetallic compounds.[10,15−17] Our work adds further results in this direction in order to better characterize the metal−metal and metal−ligand interactions and to find chemical properties that are transferable from $Mn_2(CO)_{10}$ to other complexes.

Experimental Section

Data Collection and Reduction. The commercial product was recrystallized from a light petroleum solution under CO atmosphere, and light-yellow crystals were obtained; a spherical crystal of diameter 0.51 mm was put into a Lindemann glass capillary. The intensity data were collected on a Siemens P4 diffractometer equipped with a N_2 gas stream low-temperature device. The crystal was cooled to 120 K in nearly 3 h. A total of 20 507 reflections were collected up to $2\theta = 110°$ (limiting indices $-39 < h < 39$, $-16 < k < 15$, $-32 < l < 32$), with graphite-monochromatized Mo Kα radiation ($\lambda = 0.710\,73$ Å), with a $\theta-2\theta$ scan method (scan width = 2.0°), and with variable scan speed (2.02−14.65 deg/min). Two standard reflections were measured every 50 reflections, and no crystal decay occurred. Data reduction was made using P3 and SHELXS programs.[18] The independent reflections were 8711 ($R_{int} = \sum||F_o|^2 - |F_o|^2(\text{mean})|/\sum|F_o|^2 = 0.033$, $R_\sigma = \sum[\sigma(|F_o|^2)]/\sum[|F_o|^2] = 0.039$). The crystal data are collected in Table 1.

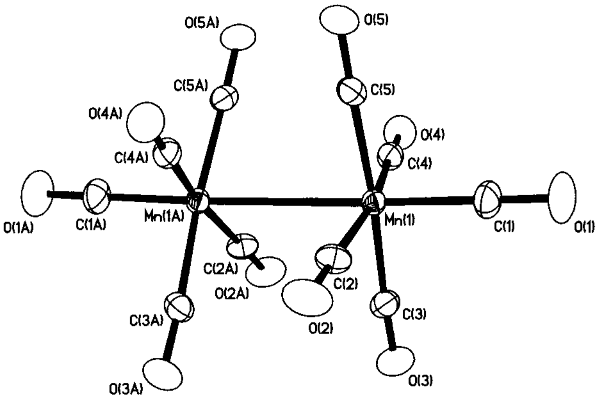

Figure 1. ORTEP plot (30% probability) of the molecule of $Mn_2(CO)_{10}$.

Table 2. IAM and Multipole Refinement Results

N_o (no. reflections)	6217	
refinement method	IAM	POP
N_p (no. parameters)	100	290
$R(F) = \sum||F_o| - k|F_c||/\sum|F_o|$	0.0427	0.0326
$wR(F) = [\sum w(|F_o| - k|F_c|)^2/\sum w|F_o|^2]^{1/2}$	0.0353	0.0216
$R(F^2) = \sum||F_o|^2 - k^2|F_c|^2|/\sum|F_o|^2$	0.0597	0.0424
$wR(F^2) = [\sum w(|F_o|^2 - k^2|F_c|^2)^2/\sum w|F_o|^4]^{1/2}$	0.0679	0.0403
$S = [\sum w(|F_o|^2 - k^2|F_c|^2)^2/(N_o - N_p)]^{1/2}$	2.005	1.209
k (scale factor)	0.2360(2)	0.2477(5)
(shift/esd)$_{max}$	< 0.02	< 0.02

Conventional X-ray Diffraction Study. The structure of $Mn_2(CO)_{10}$ was refined first by a full-matrix least-squares method using the spherical independent atom model (IAM). The corresponding scattering factors and anomalous scattering correction for Mn atoms were taken from International Tables for Crystallography (1995, Vol. C). The data were corrected for absorption effects; no correction was made for extinction because this was negligible, anomalous dispersion being considered only for the Mn atom. The atomic displacements were modeled using the anisotropic harmonic approximation. All refinements were carried out using the VALRAY program implemented by Stewart and Spackman;[19] the quantity minimized was $\sum w(|F_o|^2 - k^2|F_c|^2)^2$ based on 6217 independent reflections with $I > 2\sigma(I)$ and weights $w = 1/\sigma^2(F_o^2)$. Agreement factors and other information on data processing are given in Table 2.

An ORTEP plot of the molecule is shown in Figure 1.

Multipole Analysis. The same X-ray data of $Mn_2(CO)_{10}$ were also fitted to the aspherical atom formalism developed by Stewart.[13] The adopted rigid pseudoatom model (POP) is the following. The nucleus and the spherical core electron density correspond to the IAM, and the deformation density is a sum of terms expressed by $C_{nlm}R_n(r)Y_{lm}(\theta,\varphi)$, where C_{nlm} is a population parameter, $R_n(r)$ is a radial function of Slater type or a fixed linear combination of exponentials, and $Y_{lm}(\theta,\varphi)$ is a surface spherical harmonic. Monopole deformation has spherical symmetry and confers a net charge on the pseudoatom. All higher (than monopole) multipole terms cause aspherical deformations of the pseudoatom. A single parameter was refined for the core of all C and O atoms. On the manganese atom position functional expansions up to hexadecapole level were introduced, whereas the expansions were truncated at octapole level for the carbon and oxygen atoms. For manganese, oxygen, and carbon the core and valence monopole scattering factors were calculated from Hartree−Fock atomic wave functions.[20] For the higher multipoles the Slater type exponents (α's) of O and C atoms were assigned fixed values based on theory and the α's of manganese were determined by the least-squares method. To test the effect of the anharmonicity in thermal motion, we introduced third-order Gram−Charlier[21] coefficients in the least-squares method. The introduction of anharmonic parameters led only to a marginal drop in the R factor and no significant improvement in the multipole analysis, so they were excluded from the final model. Information on multipole refinement is given in Table 2. Hirshfeld's rigid bond test,[22] applied in an analysis of the atomic displacement parameters, was positive for all bonds (the rms is 1.0×10^{-3} Å).

---

(13) (a) MacDougall, P. J.; Hall, M. B. *Trans. Am. Crystallogr. Assoc.* **1990**, *26*, 105−123. (b) Low, A. A.; Kunze, K. L.; MacDougall, P. J.; Hall, M. B. *Inorg. Chem.* **1991**, *30*, 1079−1086.

(14) (a) Bianchi, R.; Gatti, C.; Adovasio, V.; Nardelli, M. *Acta Crystallogr.* **1996**, *B52*, 471−478. (b) Smith, G. T.; Mallinson, P. R.; Frampton, C. S.; Farrugia, L. J.; Peacock, R. D.; Howard, J. A. K. *J. Am. Chem. Soc.* **1997**, *119*, 5028−5034. (c) Iversen, B. B.; Larsen, F. K.; Figgis, B. N.; Reynolds, P. A. *J. Chem. Soc., Dalton Trans.* **1997**, 2227−2240. (d) Macchi, P.; Proserpio, D. M.; Sironi, A. *J. Am. Chem. Soc.* **1998**, *120*, 1447−1455. (e) Palmer, A.; Jauch, W. *Phys. Rev. B* **1993**, *48*, 10304−10310. (f) Lee, C. R.; Wang, C. C.; Chen, K. C.; Lee, G. H.; Wang, Y. *J. Phys. Chem. A* **1999**, *103*, 156−165. (g) Hwang, T. S.; Wang, Y. *J. Phys. Chem. A* **1998**, *102*, 3726−3731. (h) Wang, C. C.; Wang, Y.; Liu, H. J.; Lin, K. J.; Chou, L. K.; Chan, K. S. *J. Phys. Chem. A* **1997**, *101*, 8887−8901.

(15) Bianchi, R.; Gervasio, G.; Marabello, D.; Markó, L. *Atti Congr. Naz. Assoc. It. Cristallogr.* **1996**, P-122.

(16) Macchi, P.; Proserpio, D. M.; Sironi, A. *J. Am. Chem. Soc.* **1998**, *120*, 13429−13435.

(17) Jansen, G.; Schubart, M.; Findeis, B.; Gade, L. H.; Scowen, I.; McPartlin, M. *J. Am. Chem. Soc.* **1998**, *120*, 7239−7251.

(18) Sheldrick, G. M. *SHELXTL IRIS*; Siemens Analytical X-ray Instruments Inc.: Madison, WI, 1990.

(19) Stewart, R. F.; Spackman, M. A. *VALRAY User's Manual*; Department of Chemistry, Carnegie-Mellon University: Pittsburgh, PA, 1983.

(20) Clementi, E.; Roetti, C. *At. Data Nucl. Data Tables* **1974**, *14*, 177−478.

(21) Johnson, C. K.; Levy, H. A. *International Tables of X-ray Crystallography*; Kynoch Press: Birmingham, U.K. 1974; Vol. IV, pp 311−316.

(22) Hirshfeld, F. L. *Acta Crystallogr., Sect. A* **1976**, *32*, 239−244.

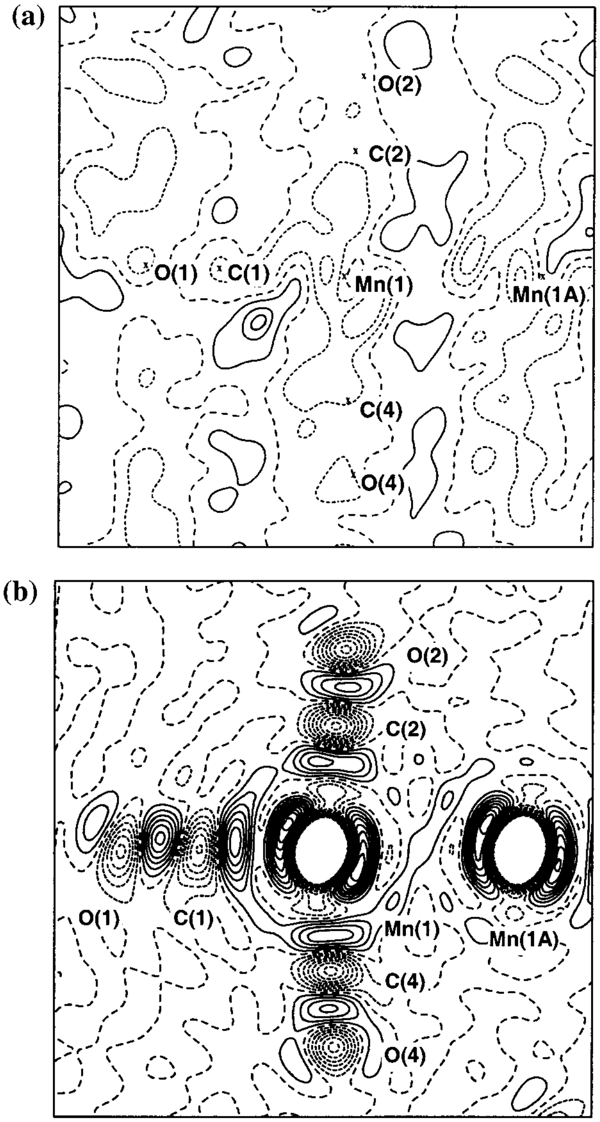

Figure 2. (a) Residual density and (b) model deformation density maps in the plane defined by Mn(1), Mn(1A), and C(2) atoms. The contour interval is 0.10 e Å^{-3}. Solid lines represent positive contour, short dashed lines represent negative contour, and the wide dashed line represents zero contour.

Table 3. Net Atomic Charges (*e*) from the Multipole Refinement

atom	charge (esd's)
Mn(1)	−0.2(3)
C(1)	−0.11(5)
O(1)	0.16(5)
C(2)	0.09(4)
O(2)	0.13(3)
C(3)	−0.26(5)
O(3)	0.12(4)
C(4)	−0.14(4)
O(4)	0.15(3)
C(5)	−0.16(4)
O(5)	0.23(3)

The largest peak (close to the Mn and C(1) nuclei) in the residual map (Figure 2a) (based on $F_{\mathrm{observed}} - F_{\mathrm{multipole}}$) is 0.33 e Å^{-3} and shows no significant features. A list of all refined parameters is given as Supporting Information. Net atomic charges, defined as the atomic number *Z* minus the sum of the core and valence populations, are given in Table 3.

The model deformation density map (Figure 2b) shows the electron accumulation due to bonding between the atoms.

We observe a slightly positive and not statistically significant deformation density around the midpoint of the Mn−Mn bond (0.1(1) e Å^{-3}) as found in ref 8a. Moreover, the deformation map shows significant maxima, midway between the other bonded atoms.

The atomic fractional coordinates and the anisotropic thermal parameters of the multipolar refinement are listed in Table 4.

Results and Discussion

Structural Properties. The well-known $Mn_2(CO)_{10}$ molecule has a crystallographic C_2 symmetry, the 2-fold axis passing through the middle of the Mn−Mn bond. Each Mn atom links four equatorial carbonyls and one axial in a pseudo-octahedral environment. The equatorial carbonyls of the two $Mn_2(CO)_5$ groups are staggered (for instance, the angle between the CO(1)−Mn(1)−CO(2) and CO(1A)−Mn(1A)−CO(2A) planes is 51°). As has already been observed in a previous paper[8a] and references therein, three equatorial carbonyls on each Mn atom are bent slightly toward the opposite manganese, and the axial Mn−C bonds are shorter than the equatorial bonds (see Table 5). The shortening of the axial Mn−C bonds is probably due to the weaker trans effect of the Mn−Mn bond. The thermal motion of the axial carbonyls is greater than that of the equatorial carbonyls probably because the steric hindrance is less (see Table 4).

The Mn(1)−Mn(1A) bond distance is 2.9042(8) Å; as expected, this value falls between the corresponding values obtained at room temperature (2.923(3) Å) and at 74 K (2.8950(6) Å), respectively.[8a]

Table 5 also lists the intermolecular van der Waals O···O and C···O contacts, which are less than 3.4 Å.

Topological Analysis. The relation between the topology of the electron density, $\rho(\mathbf{r})$, and its Laplacian, $\nabla^2\rho(\mathbf{r})$, and chemical concepts is quantified by the quantum theory of atoms in molecules (QTAM).[11] The definition of the chemical bond is based on the existence of a (3,−1) critical point (CP), defined by $\mathbf{r}_c$, along a line of maximum density (bond path) linking the nuclei of neighboring atoms. At the bond CP the gradient of the density vanishes, $\nabla\rho(\mathbf{r}) = 0$, and the sum of the three eigenvalues (two negative, λ_1 and λ_2, and one positive, λ_3) of the density Hessian matrix yields the Laplacian, $\nabla^2\rho(\mathbf{r})$. The topology of the $\nabla^2\rho(\mathbf{r})$ allows the study of localized bonding and nonbonding pairs and the characterization of local concentrations ($\nabla^2\rho(\mathbf{r}) < 0$) of the electron density and its depletion ($\nabla^2\rho(\mathbf{r}) > 0$). The number and properties of the local $\nabla^2\rho(\mathbf{r})$ maxima and minima in the valence shell charge concentration (VSCC) of the bonded atoms depend on the linked atoms themselves. In interactions where $\nabla^2\rho(\mathbf{r}_c) < 0$ ("shared" interactions), there is a lowering of the potential energy density $V(\mathbf{r})$ associated with a concentration in charge between the nuclei along the bond path. "Closed-shell" interactions, where $\nabla^2\rho(\mathbf{r}_c) > 0$, are dominated by the kinetic energy density $G(\mathbf{r})$ in the region of the interatomic surface. Additional information about chemical bond type is available from the total electronic energy density $E^e(\mathbf{r}_c) = G(\mathbf{r}_c) + V(\mathbf{r}_c)$ at $\mathbf{r}_c$. In general, atomic interactions can thus be characterized by $\rho(\mathbf{r}_c) \equiv \rho_b$, $\nabla^2\rho(\mathbf{r}_c) \equiv \nabla^2\rho_b$, $V(\mathbf{r}_c) \equiv V_b$, $G(\mathbf{r}_c) \equiv G_b$, $G(\mathbf{r}_c)/\rho(\mathbf{r}_c) \equiv G_b/\rho_b$, and $E^e(\mathbf{r}_c) \equiv E^e{}_b$ values.[11b]

The theoretical and experimental G_b and V_b values, reported in this paper, were calculated from Abramov[23] and Espinosa et al.[24] The Abramov estimate of G_b is within 4% of the high-quality Hartree−Fock values for kinetic energy densities at bond critical points of systems with "closed-shell" interactions,

---

(23) Abramov, Yu. A. *Acta Crystallogr.* **1997**, *A53*, 264−272.

(24) Espinosa, E.; Molins, E.; Lecomte, C. *Chem. Phys. Lett.* **1998**, *285*, 170−173.

Table 4. Atomic Fractional Coordinates and Anisotropic Thermal Parameters ($Å^2 \times 10^2$) from the Multipole Refinement[a]

atom	x	y	z	U_{11}	U_{12}	U_{13}	U_{22}	U_{23}	U_{33}
Mn(1)	0.06894(3)	0.73632(8)	0.22326(3)	1.770(5)	0.362(4)	1.236(4)	1.766(5)	0.346(4)	1.890(5)
C(1)	0.16145(7)	0.7450(2)	0.19989(9)	3.00(4)	1.01(3)	2.93(3)	3.69(4)	1.02(3)	4.36(4)
O(1)	0.2211(1)	0.7517(4)	0.1879(2)	4.71(8)	1.95(8)	5.35(8)	6.8(1)	2.01(9)	7.8(1)
C(2)	0.14901(6)	0.6192(1)	0.37069(7)	2.08(3)	0.14(2)	0.85(2)	2.17(3)	0.41(2)	2.05(3)
O(2)	0.19931(9)	0.5468(2)	0.46111(9)	2.84(4)	0.08(3)	0.42(3)	3.09(4)	0.85(3)	2.48(3)
C(3)	0.02443(6)	0.4957(1)	0.15177(6)	3.10(3)	0.42(3)	1.67(2)	2.06(3)	0.06(2)	2.21(2)
O(3)	−0.0029(1)	0.3518(2)	0.1024(1)	5.01(6)	0.12(4)	2.53(4)	2.38(4)	−0.50(4)	3.30(4)
C(4)	−0.02877(6)	0.8437(1)	0.07843(6)	2.50(3)	0.51(2)	1.39(2)	2.40(3)	0.57(2)	1.95(2)
O(4)	−0.08929(9)	0.9055(2)	−0.01173(9)	3.26(5)	0.96(4)	1.58(3)	3.80(5)	1.12(3)	2.38(3)
C(5)	0.10136(5)	0.9812(1)	0.29166(6)	1.84(2)	0.07(2)	1.32(2)	1.80(3)	0.22(2)	2.62(3)
O(5)	0.12107(7)	1.1329(2)	0.3315(1)	2.48(4)	−0.19(3)	1.60(3)	2.00(3)	0.01(3)	3.63(4)

[a] The temperature factor is given by $\exp[-2\pi^2(U_{11}h^2a^{*2} + ... + 2U_{23}klb^*c^*)]$.

Table 5. Bond Distances and Angles and Intermolecular van der Waals O···O and C···O Contacts Less Than 3.4 Å from the Multipole Refinement

intramolecular bonds		intermolecular contacts	
bond distance (Å)		contact distance (Å)[a]	
Mn(1)−Mn(1A)	2.9042(8)	O(1)···O(4)$^{\mathrm{I}}$	3.188
Mn(1)−C(1)	1.8199(16)	O(1)···O(5)$^{\mathrm{II}}$	3.018*
Mn(1)−C(2)	1.8537(8)	O(2)···O(2)$^{\mathrm{III}}$	3.135*
Mn(1)−C(3)	1.8525(10)	O(2)···O(5)$^{\mathrm{IV}}$	3.217*
Mn(1)−C(4)	1.8524(7)	O(2)···O(5)$^{\mathrm{III}}$	2.972*
Mn(1)−C(5)	1.8571(9)	O(3)···O(4)$^{\mathrm{V}}$	3.129*
C(1)−O(1)	1.1438(35)	O(3)···O(5)$^{\mathrm{IV}}$	2.999*
C(2)−O(2)	1.1402(12)	O(3)···O(5)$^{\mathrm{VI}}$	3.102*
C(3)−O(3)	1.1397(15)	O(4)···O(4)$^{\mathrm{I}}$	3.184*
C(4)−O(4)	1.1383(11)	O(2)···C(2)$^{\mathrm{III}}$	3.217
C(5)−O(5)	1.1390(13)	O(2)···C(5)$^{\mathrm{III}}$	3.106
		O(3)···C(4)$^{\mathrm{V}}$	3.212
bond angle (deg)		O(3)···C(5)$^{\mathrm{IV}}$	3.336
Mn(1A)−Mn(1)−C(1)	175.89(7)	O(4)···C(1)$^{\mathrm{I}}$	3.230*
Mn(1A)−Mn(1)−C(2)	83.43(4)	O(4)···C(4)$^{\mathrm{I}}$	3.220
Mn(1A)−Mn(1)−C(3)	90.20(4)	C(2)$^{\mathrm{IV}}$···O(5)	3.386
Mn(1A)−Mn(1)−C(4)	86.46(4)	C(3)$^{\mathrm{IV}}$···O(5)	3.224
Mn(1A)−Mn(1)−C(5)	84.48(4)		
C(1)−Mn(1)−C(2)	94.10(5)		
C(1)−Mn(1)−C(3)	93.10(6)		
C(1)−Mn(1)−C(4)	96.13(5)		
C(1)−Mn(1)−C(5)	92.31(5)		
Mn(1)−C(1)−O(1)	178.38(15)		
Mn(1)−C(2)−O(2)	178.96(14)		
Mn(1)−C(3)−O(3)	175.91(13)		
Mn(1)−C(4)−O(4)	178.40(9)		
Mn(1)−C(5)−O(5)	178.48(12)		

[a] The roman numbers refer to the following symmetry operations. I: $-x, 2 - y, -z$. IV: $x - 1, y, z$. II: $0.5 - x, y - 0.5, 0.5 - z$. V: $-x, 1 - y, -z$. III: $0.5 - x, 1.5 - y, 1 - z$. VI: $-x, y - 1, 0.5 - z$. Contacts marked with an asterisk indicate atomic interactions where bond paths and CP's were found from the topological analysis of the experimental $\rho(\mathbf{r})$ (see Table 7).

whereas molecules with “shared” interactions are only in semiquantitative agreement (up to 27%) with the theoretical values. Furthermore, the experimental electron density is affected by systematic errors due to thermal atomic motion in crystals and the use of the truncated set of observed structure factors. These errors must also be taken into account in G_b estimation.[23] When the G_b and V_b magnitudes are nearly equal (e.g., in ionic interactions) the calculation of E^e_b is subject to further error due to subtractive cancellation.

Theoretical values of ρ_b, $\nabla^2\rho_b$, G_b, G_b/ρ_b, V_b, and E^e_b for some covalent and ionic interactions, reported in the literature,[25] are illustrated in Table 6.

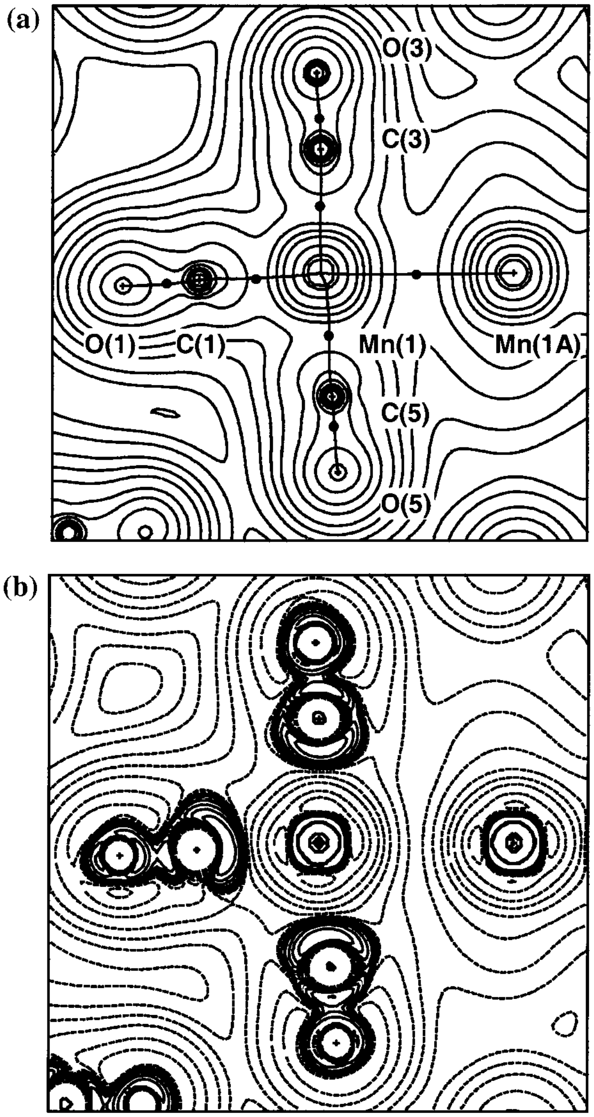

Figure 3. Experimental electron density, $\rho(\mathbf{r})$ (a) and its Laplacian, $\nabla^2\rho(\mathbf{r})$, (b) on the plane defined by Mn(1), Mn(1A), and C(3) atoms. The absolute values of the contours (au) increase from the outermost one inward in steps of 2×10^n, 4×10^n, and 8×10^n with n beginning at -3 and increasing in steps of 1. In the electron density map (a) the pair of trajectories (bond path) of $\nabla\rho(\mathbf{r})$ that originate at bond CP are superimposed on the same map. In the $\nabla^2\rho(\mathbf{r})$ map (b) positive values are denoted by dashed contours, and negative values are denoted by solid contours.

The covalent bonds (Table 6) show relatively large values of ρ_b and large negative values of $\nabla^2\rho_b$. These “shared” interactions have negative E^e_b being dominated by large negative V_b associated with charge concentration in the internuclear region. Instead the ionic bonds have relatively low ρ_b and positive $\nabla^2\rho_b$ as the density contracts away from the contact

---

(25) Bader, R. F. W.; Essén, H. *J. Chem. Phys.* **1984**, *80*, 1943−1959.

Table 6. Theoretical Bond Critical Point Data for Covalent and Ionic Binuclear Interactions[25]

	ρ_b (e Å^{-3})	$\nabla^2\rho_b$ (e Å^{-5})	G_b (hartree Å^{-3})	G_b/ρ_b (hartree e^{-1})	V_b (hartree Å^{-3})	E^e_b (hartree Å^{-3})
Covalent Interaction						
H_2	1.8408	−33.2178	0.6730	0.3656	−3.6715	−2.9985
N_2	4.8714	−73.5013	7.8259	1.6064	−20.7973	−12.9715
NO	4.0036	−49.0483	5.8277	1.4556	−15.0892	−9.2615
O_2	3.7202	−24.4048	6.0430	1.6243	−13.7945	−7.7515
CC bond in ethylene	2.4475	−28.6583	2.2367	0.9138	−6.4796	−4.2430
CH bond in CH_4	1.8692	−23.5783	1.1802	0.6314	−4.0112	−2.8309
OH bond in H_2O	2.6378	−58.8396	1.3031	0.4940	−6.7255	−5.4223
Ionic Interaction						
LiCl	0.3118	6.4030	0.4141	1.3282	−0.3799	0.0342
NaCl	0.2416	4.8294	0.3007	1.2448	−0.2634	0.0373
NaF	0.3698	11.2180	0.6768	1.8300	−0.5682	0.1086
KF	0.3738	7.5477	0.5083	1.3595	−0.4881	0.0201
MgO	0.6093	15.6787	1.0839	1.7787	−1.0702	0.0137

Table 7. Bond Critical Point Properties for $Mn_2(CO)_{10}$[a]

X−Y	R_e (Å)	R_b (Å)	R_x (Å)	ρ_b (e Å^{-3})	$\nabla^2\rho_b$ (e Å^{-5})	λ_1 (e Å^{-5})	λ_2 (e Å^{-5})	λ_3 (e Å^{-5})	G_b (hartree Å^{-3})	G_b/ρ_b (hartree e^{-1})	V_b (hartree Å^{-3})	E^e_b (hartree Å^{-3})
Intramolecular Interaction												
Mn(1)−Mn(1A)	2.9042(8)	2.9054	1.4527	0.190(4)	0.815(8)	−0.197(3)	−0.197(3)	1.209(6)	0.088	0.466	−0.120	−0.031
			1.452	0.143	0.674	−0.164	−0.156	0.995	0.063	0.440	−0.079	−0.016
Mn(1)−C(1)	1.820(1)	1.822	0.932	1.06(2)	16.1(3)	−4.40(5)	−3.97(5)	24.5(3)	1.64	1.54	−2.15	−0.51
			0.841	0.77	9.4	−3.53	−3.51	16.5	0.96	1.24	−1.26	−0.30
Mn(1)−C(2)	1.8537(8)	1.9080	0.9248	0.66(2)	14.3(3)	−2.50(5)	−1.18(5)	18.0(3)	1.07	1.62	−1.14	−0.07
			0.863	0.72	8.9	−3.21	−3.18	15.3	0.88	1.22	−1.14	−0.26
Mn(1)−C(3)	1.853(1)	1.866	0.935	0.85(2)	14.5(2)	−3.81(3)	−2.55(3)	20.9(2)	1.29	1.51	−1.56	−0.27
			0.863	0.72	8.9	−3.22	−3.18	15.3	0.88	1.22	−1.14	−0.26
Mn(1)−C(4)	1.8524(7)	1.9075	0.9504	0.78(2)	11.8(2)	−4.37(3)	−2.89(3)	19.1(2)	1.08	1.39	−1.34	−0.26
			0.863	0.72	8.9	−3.23	−3.18	15.3	0.88	1.22	−1.14	−0.26
Mn(1)−C(5)	1.8571(9)	1.8800	0.9419	0.85(2)	13.3(2)	−4.13(3)	−2.92(3)	20.3(2)	1.23	1.45	−1.54	−0.30
			0.866	0.71	8.8	−3.18	−3.15	15.2	0.86	1.22	−1.11	−0.25
C(1)−O(1)	1.144(4)	1.148	0.406	3.69(9)	−45(5)	−44(3)	−43(3)	42(5)	5.0	1.4	−13.1	−8.1
			0.747	2.43	34	−16	−16	66	5.1	2.1	−7.9	−2.7
C(2)−O(2)	1.140(1)	1.142	0.407	3.25(8)	−24(3)	−36(2)	−32(2)	44(2)	4.6	1.4	−10.9	−6.3
			0.745	2.44	35	−16	−16	68	5.2	2.1	−7.9	−2.7
C(3)−O(3)	1.140(2)	1.142	0.436	3.57(7)	−44(2)	−36(1)	−33(1)	25(1)	4.6	1.3	−12.4	−7.7
			0.744	2.45	35	−16	−16	68	5.2	2.1	−8.0	−2.8
C(4)−O(4)	1.138(1)	1.140	0.419	3.36(7)	−32(2)	−34(1)	−31(1)	33(1)	4.6	1.4	−11.4	−6.8
			0.744	2.45	36	−16	−16	69	5.3	2.1	−8.0	−2.7
C(5)−O(5)	1.139(1)	1.139	0.451	3.83(7)	−57(2)	−42(1)	−39(1)	24(1)	4.9	1.3	−13.7	−8.9
			0.744	2.45	36	−16	−16	69	5.3	2.1	−8.0	−2.7
Intermolecular Interaction												
O(1)···O(5)^{II}	3.018	3.027	1.500	0.039(1)	0.68(1)	−0.018	−0.001	0.173	0.04	0.9	−0.02	0.02
O(2)···O(2)^{III}	3.135	3.164	1.568	0.045(1)	0.63(1)	−0.108	−0.017	0.758	0.04	0.8	−0.02	0.02
O(2)···O(5)^{IV}	3.217	3.452	1.568	0.030(1)	0.43(1)	−0.072	−0.028	0.534	0.02	0.7	−0.01	0.01
O(2)···O(5)^{III}	2.972	3.082	1.455	0.052(1)	0.79(1)	−0.143	−0.064	1.000	0.04	0.8	−0.03	0.01
O(3)···O(4)^{V}	3.129	3.448	1.515	0.042(1)	0.59(1)	−0.097	−0.045	0.730	0.03	0.7	−0.02	0.01
O(3)···O(5)^{IV}	2.999	3.026	1.520	0.048(1)	0.74(1)	−0.130	−0.066	0.932	0.04	0.8	−0.03	0.01
O(3)···O(5)^{VI}	3.102	3.108	1.566	0.032(1)	0.55(1)	−0.088	−0.072	0.713	0.03	0.9	−0.02	0.01
O(4)···O(4)^{I}	3.184	3.184	1.592	0.046(1)	0.64(1)	−0.113	−0.012	0.767	0.03	0.7	−0.02	0.01
O(4)···C(1)^{I}	3.230	3.235	1.530	0.038(1)	0.48(1)	−0.091	−0.031	0.598	0.03	0.7	−0.02	0.01

[a] R_e = distance between atoms X and Y; R_b = bond path length; R_x = distance (Å) between atom X and the bond critical point. First row from POP model and second row from IAM model.

region of the interacting atoms. These "closed-shell" interactions are dominated by the kinetic energy in the region of the bond CP, G_b being slightly greater than $|V_b|$ and the energy density ($E^e_b > 0$) close to zero.

Figure 3 shows the experimental electron density of $Mn_2(CO)_{10}$ and its Laplacian in the plane containing the two metal atoms, and the CO(1), CO(3), and CO(5) carbonyls.

As mentioned above, three of the equatorial carbonyls on each Mn atom are bent slightly toward the other Mn atom, but there appears to be no bond path between the metal atom and the equatorial carbonyls of the other $Mn(CO)_5$ group, thus ruling out any cross-interaction that might be responsible for the said bending of the three equatorial carbonyls.

The results of the topological analysis of the experimental electron density of $Mn_2(CO)_{10}$ are reported in Table 7.

(a) C−O Bonds. The C−O bonds are characterized (Table 7) by high values of ρ_b and large negative values of $\nabla^2\rho_b$ (3.54 e Å^{-3} ave and −40 eÅ^{-5} ave, respectively), in agreement with the values for the covalent bonds shown in Table 6. Similar experimental values of ρ_b and of $\nabla^2\rho_b$ can be found elsewhere.[16] The trend of the ρ_b values does not support a systematic difference in strength between the CO_{ax} and the CO_{eq} bonds. However, the IR spectra reveal significantly different values for the force constants[8b] (16.308 × 10^{-8} N Å^{-1} for CO_{ax} and 16.500 × 10^{-8} N Å^{-1} for CO_{eq}). The average ρ_b value of the CO bonds is in good agreement with the theoretical one for the

Table 8. Bond Critical Point Data from Experimental Electron Density of Some Metal Complexes[a]

complex	bond	ρ_b (e Å^{-3})	$\nabla^2\rho_b$ (e Å^{-5})	G_b (hartree Å^{-3})	G_b/ρ_b (hartree e^{-1})	V_b (hartree Å^{-3})	$E^e{}_b$ (hartree Å^{-3})	ref
$Co(NO_2)_6Li[N(CH_3)_4]_2$	Co−N	0.56(1) ave	12.6(1) ave	0.89	1.60	−0.90	−0.012	14a
$(NiH_3L)(NO_3)(PF_6)$[a]	Ni−N	3.10(9)	1.4(3)	5.36	1.73	−10.6	−5.27	14b
	Ni−O	0.93(4)	9.77(7)	1.17	1.26	−1.65	−0.48	
$Ni(ND_3)_4(NO_2)_2$	Ni−N	0.65(2)	7.1(2)	0.72	1.11	−0.95	−0.23	14c
	Ni−N	0.76(5)	9.9(3)	0.97	1.28	−1.25	−0.28	
$Ni(COD)_2$	Ni−C	0.545(8) ave	4.98(7)	0.52	0.96	−0.70	−0.18	14d
$Co_2(CO)_6(AsPh_3)_2$	Co−CO	0.93(2) ave	12.25(2)	1.27	1.38	−1.71	−0.42	16
	Co−As	0.46(1) ae	4.23(2)	0.42	0.91	−0.54	−0.13	
	As−C	0.84(1) ave	2.750(9)	0.71	0.86	−1.27	−0.54	
$Mn_2(CO)_{10}$	Mn−CO	0.84(2) ave	14.0(2)	1.26	1.50	−1.55	−0.28	this work

[a] H_3L = *N*,*N*′,*N*″-Tris(2-hydroxy-3-methylbutyl)-1,4,7-triazacyclononane.

CO molecule[11] (3.54_{exp} versus 3.42_{theor} e Å^{-3}), while the theoretical $\nabla^2\rho_b$ value is different and, contrary to the experimental value, is positive (24.0 e Å^{-5}). Table 7 shows the values of ρ_b and $\nabla^2\rho_b$ for the promolecule. It can be seen that they are completely different from the corresponding values of the POP model, whereas they are similar to the values of the "closed-shell" interactions. The promolecule does not describe the covalent bonds correctly.

For each CO group the bond-CP is closer to the carbon nucleus (C−CP = 0.424 Å ave) than to the oxygen, indicating that the C atom accumulates less electronic charge in the vicinity of its nucleus. For the CO molecule this effect is more pronounced; in fact the theoretical C−CP distance is shorter (0.375 Å).[11a] The VSCC analysis of the O atoms shows a maximum along each C−O bond path at a mean distance of 0.718 Å from the oxygen nucleus.

The C−O bonds are characterized by large negative $E^e{}_b$ values as the potential energy density contribution ($V_b = -12.3$ hartree Å^{-3} ave) predominates over the positive electronic kinetic energy density contribution ($G_b = 4.7$ hartree Å^{-3} ave). The negative $E^e{}_b$ values for these bonds denote their "shared" character, in agreement with the trend of the covalent interactions shown in Table 6.

(b) Mn−C Bonds. The ρ_b values for Mn−C bonds are lower than for C−O bonds, approximately by a factor 5.0. This further supports the IR analysis results concerning the strength of the Mn−C and C−O bonds. In fact, the force constants of these bonds are 2×10^{-8} and 16.4×10^{-8} N Å^{-1} ave, respectively.[8b,d] All the Mn and C atoms are linked by a bond path, and their bond CP's lie close to the middle point between the interacting atoms. The Mn−C(1) bond differs significantly from the other Mn−C bonds in the bond distance (1.820(2) Å versus 1.854(1) ave Å) and in the value of ρ_b (1.06 e Å^{-3} versus 0.79 e Å^{-3} ave). The $\nabla^2\rho_b$ values for Mn−C bonds are positive, and each C atom has a VSCC maximum directed toward the metal atom at an average distance of 0.450 Å from the C nucleus. The Laplacian of the electron density (see Figure 3b) is positive in the neighborhood of the bond critical point between the metal and the CO ligands. For the Mn−C bonds, ρ_b (0.73 e Å^{-3} ave) and $\nabla^2\rho_b$ (9.0 e Å^{-5} ave) of the IAM model are quite close to the corresponding values (0.84 e Å^{-3} ave and 14.0 e Å^{-5} ave, respectively) of the POP model. The G_b and $|V_b|$ values are almost comparable, $|V_b|$ prevailing and resulting in energy densities $E^e{}_b$ with slightly negative values. In conclusion, the interactions considered until now have exhibited ρ_b, $\nabla^2\rho_b$, G_b, V_b, and $E^e{}_b$ values intermediate to those characteristic of the two limiting types of interactions shown in Table 6, close to the values of ionic interactions. Table 8 lists the experimental values of ρ_b, $\nabla^2\rho_b$, G_b, V_b, and $E^e{}_b$ of some Lewis acid−base interactions in a number of complexes, where the metal is a transition element with a zero (refs 14d, 16, and this work) or positive (ref 14a−c) oxidation number and the ligand is neutral or anionic.

The values of the topological parameters (except for Ni−N in ref 14b) at the bond CP are close to the corresponding ones of $Mn_2(CO)_{10}$ (see Table 8); therefore, these values appear to be typical of a Lewis acid−base dative bond. The same trend was observed by Frenking et al.[26] for a number of adducts between BX_3 (X = F, Cl) and Lewis bases and in other metal complexes.[14f−h] The Mn−C interactions have properties that bridge those of the ionic systems at the "closed-shell" limit and those of the covalent and polar-covalent systems of the "shared" interactions.

(c) Mn−Mn Bond. The Mn−Mn bond path (Figure 3a) connecting the two $Mn(CO)_5$ moieties exhibits small and positive ρ_b (0.190(4) e Å^{-3}) and $\nabla^2\rho_b$ (0.815(8) e Å^{-5}) values (see Table 7), close to the corresponding theoretical values (ρ_b = 0.209 e Å^{-3} and $\nabla^2\rho_b = -0.144$ e Å^{-5}) calculated by MacDougall.[7i] This result is in keeping with the low force constant (0.59×10^{-8} N Å^{-1}) reported in the literature.[8e,f] No (3,−3) CP (corresponding to the theoretical pseudoatom) was detected near the middle point of the Mn−Mn bond, as found in the theoretical electron density distribution of some lithium or sodium clusters.[27] Moreover, theoretical studies of some close-packed transition metals[28] show that low electron density and positive Laplacian at the bond CP are typical of the metallic bonding.

The G_b and $|V_b|$ values are small, and the negative energy density ($E^e{}_b = -0.031$ hartree Å^{-3}) is very close to zero. With respect to Mn−C bonds (Table 7), the topological parameters of the Mn−Mn bond are closer to those of the IAM model and show a trend close to *ionic* interactions (see Table 6).

Around the Mn atom we found six nonbonded VSCC maxima at a distance of 0.342 Å ave, arranged at the vertexes of a highly distorted octahedron and with the carbonyl ligands and the other Mn atom capping six faces. It is interesting to note that these VSCC maxima of the metal atom avoid, as far as possible, the datively bonded charge concentrations of the carbon atoms. Repulsion of the metal electron clouds from ligands is in accordance with the crystal field theory.

Atomic Charges. The charge values reported in Table 3 depend on the chosen multipole model used to represent the

---

(26) Jonas, V.; Frenking, G.; Reetz, M. T. *J. Am. Chem. Soc.* **1994**, *116*, 8741−8753.

(27) (a) Cao, W. L.; Gatti, C.; MacDougall, P. J.; Bader, R. F. W. *Chem. Phys. Lett.* **1987**, *141*, 380−385. (b) Gatti, C.; Fantucci, P.; Pacchioni, G. *Theor. Chim. Acta* **1987**, *72*, 433−458.

(28) (a) Eberhart, M. E.; Donovan, M. M.; Outlaw, R. A. *Phys. Rev. B* **1992**, *46*, 12744−12747. (b) Eberhart, M. E.; Clougherty, D. P.; Louwen, J. N. *MRS Bull.* **1991**, *16*, 53−58. (c) Eberhart, M. E.; Donovan, M. M.; MacLaren, J. M.; Clougherty, D. P. *Prog. Surf. Sci.* **1991**, *36*, 1−34.

electron density in the crystal; also, the correlation between the multipole parameters can lead to biased parameter estimates. Nevertheless, they can be useful for a qualitative analysis of the physical and chemical properties of molecules and crystals.

As expected, the charges of $Mn_2(CO)_{10}$ indicate that the Mn atom and CO ligands can be considered neutral within experimental error ($<3\sigma$) except for the CO(2) ligand with a positive charge equal to 0.22(5) e. In this particular case, the charge of C(2) was not well determined by the least-squares method. In Table 3 the multipole charges have negative values on carbons and positive values on oxygens. There is even an inversion of polarity in the theoretical density of free carbon monoxide derived by McLean and Yoshimine.[29] The theoretical dipole moment, however, approaches the experimental value (+0.044 au) when a more extended basis is used;[30] the experimental value of the dipole moment of the free CO corresponds (conventionally) to negative and positive point charges on C and O atoms, respectively. In Figure 3b, the Laplacian field topology around the CO ligands shows that the carbon centroids of negative charge move toward the Mn atom (as discussed above), indicating the polarization sense of the CO molecules. Thus, the effect of polarization appears to prevail over the electronegativity of the atoms in the determination of the multipole charges.

Intermolecular Interactions. Nine independent bond critical points with $\rho_b = 0.041(1)$ ave (Table 7) are associated with nine O···O and O···C bond paths with the characteristics of "closed-shell" interactions ($\nabla^2\rho_b = 0.61(1)$ e Å^{-5} ave and $E^e{}_b = 0.01$ hartree Å^{-3} ave). Not for all the intermolecular contacts (<3.4 Å) reported in Table 5 a bond path was found because the electron density between the atoms involved in these contacts is very low; however, such contacts contribute to the binding of the $Mn_2(CO)_{10}$ molecules in the crystal. Most of the contacts (Table 5) are of the type O···O, and of these, the O(5) atom has the greatest number of contacts. Furthermore, there is a bond path between the C(1) and O(4) atoms that could be responsible for the deviation from linearity of the Mn(1A), Mn(1), and C(1) atoms.

The experimental cohesive energy of $Mn_2(CO)_{10}$ was −15.0 kcal mol^{-1}.[31] By use of the results of the POP multipole model and a method described by Spackman,[32] which sums intermolecular energies, the cohesive energy of $Mn_2(CO)_{10}$ was estimated to be −13.0 kcal mol^{-1}.

Conclusions

A topological analysis of the experimental electron density of $Mn_2(CO)_{10}$, the data being from accurate X-ray diffraction experiments, revealed a bond path between the two metal atoms, indicating the existence of a direct Mn−Mn bond. The quantum theory of atoms in molecules allows the characterization of the metal−metal, metal−ligand, and C−O interactions through the topological parameters at the bond critical point (i.e., ρ_b, $\nabla^2\rho_b$, G_b, V_b, $E^e{}_b$) and their classification into the two classes of "shared" and "closed-shell" interactions. On the basis of the values obtained for the mentioned topological parameters, the two types of bond, "*metallic*" and "*donor−acceptor*", can be classified between ionic and covalent bonds.

The valence electron density of the Mn atom is aspherical, and the regions of high field tend to lack electron density because of the ligands. Such a distribution conforms with the *soft* property of the Mn atom in $Mn_2(CO)_{10}$.

On passing from one bond to another, i.e., from Mn−Mn to Mn−C to C−O, the ρ_b values increase, and this is in agreement with the force constants obtained from the IR data.[33]

An examination of all the topological results considered in this paper reveals the general trend for the classification of the atomic interactions, schematized thus:

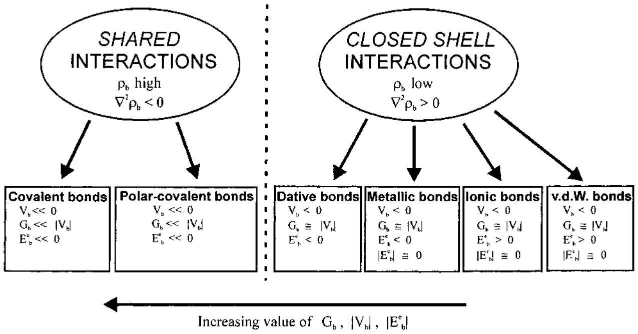

The *metallic bond* is characterized by relatively low ρ_b, G_b, and $|V_b|$ values and a positive $\nabla^2\rho_b$ value and negative $E^e{}_b$ that, being very close to zero, result in loss of precision. The parameters associated with *donor−acceptor* bonds have values close to those of the metallic bond but shifted less toward the ionic interaction. For all the interaction types there is no particular trend for the quantity G_b/ρ_b.

The proposed classification of the above bonding interactions needs confirmation by further topological studies on organometallic and coordination compounds.

Acknowledgment. The authors thank Dr. E. Diana for supplying the crystals and Dr. C. Gatti for useful discussions.

Supporting Information Available: Tables of atomic coordinates, anisotropic thermal parameters, bond lengths and angles, and multipolar population parameters. This material is available free of charge via the Internet at http://pubs.acs.org.

IC991316E

---

(29) McLean, A. D.; Yoshimine, M. Tables of linear molecular wave functions, IBM, *J. Res. Dev., Suppl.* **1967**, 11.

(30) Szabo, A.; Ostlund, N. S. *Modern Quantum Chemistry, Introduction to Advanced Electronic Structure Theory*; McMillan Publishing Co., Inc.: New York, 1982.

(31) (a) Wagman, D. D. *Nat. Bur. Stand. (U.S.), Tech. Note* **1965**, *71*, 270-1. (b) Connor, J. A.; Skinner, H. A.; Virmani, Y. *J. Chem. Soc., Faraday Trans.* **1972**, 1754−1763.

(32) (a) Spackman, M. A. *J. Chem. Phys.* **1986**, *85*, 6579−6586. (b) Spackman, M. A. *J. Chem. Phys.* **1986**, *85*, 6587−6601. (c) Spackman, M. A. *J. Chem. Phys.* **1987**, *91*, 3179−3186.

(33) Grimme, S. *J. Am. Chem. Soc.* **1996**, *118*, 1529−1534.